Response to referee comments for:

Lim et al.

"Secondary organic aerosol formation from the laboratory oxidation of biomass burning emissions"

Referee #1

Referee #1: Title: Accurate but not precise, in my opinion. Some reference could be made that this is a lab study and/or utilizes a photooxidation mini-chamber.

Author response: Title changed to "Secondary organic aerosol formation from the laboratory oxidation of biomass burning emissions" to better represent the work presented in the paper.

Referee #1: P4.20 Where/how is the additional O3 injected? Is there a sufficient jet to induce mixing? Is there any concern about a small area of highly concentrated O3 chemistry in the chamber? I'm curious about the O3/OH reactivity in general in your chamber, but more specifically at the injection port.

Author response: Ozone is generated with a pen-ray lamp external to the chamber and air carrying the O_3 is injected through a port separate from the injection port for the biomass burning emissions. The ozone concentration from the pen-ray lamp is about 1 ppm, but is mixed with humid air before injected into the chamber. The resulting O_3 concentration is approximately 200 – 300 ppb at the point of injection with a chamber mixing time of around 20 minutes. It is true that the area near the O_3 injection port will have higher O_3 concentrations relative to the rest of the bag which may lead to enhanced O_3 chemistry. However, from an experiment with no 254 nm UV, we do not observe strong changes in the composition of the aerosol with just O_3. Additionally, 254 UV makes OH in proportion to O_3, so the OH/O_3 ratio should not be sensitive to the O_3 concentration gradient in the chamber.

Referee #1: P5.2 Were seeded blanks (e.g. ammonium sulfate) ever run to establish a background OA production for this chamber and test the efficacy of the cleaning procedure?

Author response: Yes, seeded blanks (with ammonium sulfate particles) were run and showed negligible OA formation indicating that the cleaning procedure was successful. Deuterated butanol was not injected for the blanks (i.e., no OH exposure could be calculated), but O_3 and UV conditions were similar to those used in biomass burning oxidation experiments. The following text was added to the main manuscript (page 5, lines 4-5):

"*Seeded blanks (with ammonium sulfate particles) were run and showed negligible OA formation indicating that the cleaning procedure was successful.*"

Referee #1: P5.8 Did the black carbon measurements for these two methods agree? I wonder because the SP2 can saturate at high number concentrations, and the SP-AMS CE for BC requires some additional considerations (Ahern et al., 2016; Onasch et al., 2012; Willis et al., 2014.)

Author response: SP2 and SP-AMS black carbon mass loadings generally agree within a factor of two, with SP2 mass loadings consistently higher than the measurements from the SP-AMS and a reasonably linear relationship ($r^2 = 0.9$). BC measurements from the SP2 are those reported in the manuscript. The SP2 was operated with time-varying flow rates to account for the large dynamic range in the BC concentrations over the course of an experiment. In this manner, coincidence and under-counting (saturation) issues were avoided. The SP2 was calibrated with size-selected fullerene soot, and mass concentrations were corrected for "missing mass" outside of the SP2 detection window via multi-modal log-normal fitting. However we note that SP-AMS BC measurements were used only to determine which experiments to filter out of the analysis (due to enhanced wall loss), and so any CE-related errors will not affect the results presented. Black carbon measurements and other details about primary emissions will be discussed further in a future publication (Cappa et al., in preparation).

Referee #1: P5.26-30 I find your parameterization of CE very interesting and possibly broadly applicable. But why was it necessary at all? If you can calculate MFR, why not use the SEMS-measured size distribution to correct for CE directly? Given the large amount of variability in your FigS3, it is not obvious that using the correlation is an improvement in accuracy or precision over a size distribution correction. Additionally, I don't agree with the statement that there was no good internal standard available. While I think that your CE parameterization could be very useful, it warrants verification by looking at other measurements more closely. For example, you state that there was an SO2 monitor, which would allow for a sulfur mass balance. Black carbon, measured by SP-AMS or SP2, was present at useful concentrations for some of the experiments.

Author response: While an SO_2 monitor was present, we observed that the measurements were unreliable due to, most likely, strong interferences from large concentrations of PAH's and other molecules, despite the internal scrubber in the SO_2 monitor. Further, it is not entirely clear to us how sulfur balance (gas + particle) would provide clear insights into the particle collection efficiency; we did not have an independent particulate sulfate measurement, but a gas-phase sulfur measurement. Given that the SO_2 measurements were compromised by interferences, we have now removed them from the list of measurements that were made. While we can use the SEMS-determined MFR, it is not clear how this would lead to a "direct" correction for the CE. It would provide an alternative approach, but with a complication that the MFR from the SEMS would include contributions from non-refractory material and thus does not directly address the issue of how the organic component of the particles responded to temperature changes. The CE changes observed derive, in part, from changes in the organic MFR that

result from oxidation leading to less volatile OA. This would only partially be captured by the SEMS because of the contribution of non-refractory components (e.g. BC). BC cannot be used as an internal standard since the BC and organic mixing state varied dramatically between experiments, with some having the majority of the organic and BC being internally mixed (at low [OA]/[BC] ratios) and some having most of the organic material externally mixed from BC (at high [OA]/[BC] ratios) (McClure et al., *in prep.*). Given these overall issues, we believe that the organic MFR links more closely to the physical changes that occur. The text in the manuscript was amended (page 5, line 31):

"However, we were unable to find a suitable tracer in these experiments: sulfate changes as a result of oxidation of emitted SO2, black carbon (when present in high concentrations) exhibited wall losses different from OA (as described below) ***and appeared not to be homogeneously mixed with the OA (McClure et al., in prep),*** *and POA tracers (such as the C7H11+ ion, recently used by Ahern et al. (2019)) are likely to be lost via heterogeneous oxidation at the high OH exposures examined here. Thus, corrections for CE, dilution, and particle wall loss were carried out individually, as described below."*

Referee #1: P5.31 Would you please confirm that the experiments used to calculate your CE were devoid of nucleation, particles grown outside the SEMS or AMS transmission/measurement ranges, and weren't unduly influenced by rBC after thermodenuding? Also, out of curiosity, how frequently was the thermodenuder valve switched, and therefore a new CE able to be calculated?

Author response: Yes, only data that did not show significant nucleation and had low rBC loadings were used to calculate the CE parameterizations. In addition, only SEMS and PToF size distributions that could be fit to a lognormal function were used. The thermodenuder valve was switched from thermodenuder to bypass every two minutes. Some additional text clarifying these details is included in the main text (page 6, lines 4-6):

"CE and particle density were calculated by comparing AMS particle time-of-flight (PToF) and SEMS size distributions (Bahreini et al., 2005) for a subset of data points with PToF and SEMS distributions that could be fit to lognormal functions, did not show significant particle nucleation, and had low rBC concentration (see below)."

Referee #1: P6.2-3 Please provide a citation or clarify regarding the relationship between volatility and phase. It might be easier to provide citations that claim that SOA has been observed to be an amorphous solid with low volatility, and therefore is likely to bounce.

Author response: This is an excellent idea; we have included citations for Matthew et al. (2008) describing collection efficiencies as a function of particle phase in the AMS, as well as Virtanen et al. (2010) showing that SOA can be an amorphous solid.

Referee #1: P8.5 What are the possible implications for the chamber OA concentration having decreased by two orders of magnitude from the beginning to the end of the experiment (FigS4)? It stands to reason that fewer of the semi-volatile SOA products will condense at low OA concentrations late in the experiment, but that any that do condense will have a larger impact on OSc.

Author response: From Fig. S4, the organic concentration decreases by only one order of magnitude (200 μg/m^3 to 20 μg/m^3). Although semi-volatile gases are less likely to condense at low OA concentrations observed at the end of experiments due to significant dilution over the course of each experiment, most reactive gases are likely to have reacted relatively early in the experiment when dilution has less of an impact (see Fig. 6, most SOA growth occurs within ~2 days). Indeed, those gases (and potentially secondary products) that do react at longer OH exposures and condense are likely to have a large impact on the calculated average OS_C and elemental ratios of the OA. Thus, the calculated OS_C and elemental ratios may be more representative of the oxidized long-lived gases (which condense) rather than the BBOA + SOA as a whole. The following additional text was added to the manuscript to clarify this point (page 8, lines 7-8):

"*Over longer timescales, when dilution is more significant and OA concentrations are lower, calculated OS_C are likely to reflect the oxidation of longer-lived gases.*"

Referee #1: P10.18 How does this approach compare with the measured PTR-MS NMOG concentrations? It's not obvious to me why you compare [calculated VOC reacted]/[measured SOA formed] instead of [measured VOC reacted]/[measured SOA formed]? Or to go backwards, can you use your [measured NMOG reacted]* this calculated SOA yield to predict SOA formation?

Author response: We are not able to directly measure the amount of NMOG reacted, due to the dilution loss of NMOG (gases removed from the chamber before they can be reacted with OH), formation of secondary gas-phase products, and potential off-gassing of non-SOA forming low molecular weight NMOG from the chamber walls, leading to calculated SOA yields greater than unity. Thus, only initial NMOG measurements are used for the analysis and reacted NMOG are calculated as described in the text. This explanation is now included in the main text (page, lines)

Referee #1: P11.19 Given the importance of dilution and volatility on the results presented here, is there information on the volatility of the POA and the SOA from the thermodenuder measurements, that can be compared to past campaigns?

Author response: Hennigan et al. (2011) observe an increase in organic MFR (80 C) for fires that show high OA enhancement as well as fires that show low OA enhancement. We do observe a decrease in volatility with oxidation – POA is relatively

volatile, while SOA is less so. However, because we only used one temperature for the thermodenuder (250 C), we cannot obtain a volatility distribution as they do in May et al. (2013) where MFR was measured over a range of temperatures from 20 C to 120 C. Thus, comparing with either data set directly is difficult since our thermodenuder was run only at a single temperature that was much higher than the thermodenuder temperatures of the previously mentioned studies. Page 6, lines 8-9 were edited to mention that increases in MFR with oxidation are consistent with previous studies:

"Generally, POA has low organic MFR (i.e., relatively volatile) and particle MFR increases with oxidation, consistent with previous work (Hennigan et al., 2011)."

Hennigan, C J, Miracolo, M. A., Engelhart, G. J., May, A. A., Presto, A. A., Lee, T., & Sullivan, A. P. (2011). Chemical and physical transformations of organic aerosol from the photo-oxidation of open biomass burning emissions in an environmental chamber. *Atmospheric Chemistry and Physics*, 7669–7686. https://doi.org/10.5194/acp-11-7669-2011

May, Andrew A., Levin, E. J. T., Hennigan, C. J., Riipinen, I., Lee, T., Collett, J. L., et al. (2013). Gas-particle partitioning of primary organic aerosol emissions: 3. Biomass burning. *Journal of Geophysical Research Atmospheres*, 118(19), 11327–11338. https://doi.org/10.1002/jgrd.50828

Minor technical corrections:

Referee #1: P3.22 "subalpine fir" rather than "subalpine fire"

Author response: Corrected.

Referee #1: P7.25 Please include Hennigan et al. 2011

Author response: Citation now included.

Referee #1: P11.20 Missing a period.

Author response: Corrected.

Referee #1: FigS3 No red exponential fit

Author response: Red exponential fit was from an old version of the plot. Text referring to it has been removed.

Referee #1: FigS6 It looks like some plots have multiple y-values for a given time; some boomerangs at 0-5 days where they should be smooth functions. Is it possible that the d-butanol injection is also being plotted? Does this change the OA enhancement ratios?

Author response: D-butanol injection is not being plotted. The left panel of Fig. S6 is actually in units of hours to compare with Hennigan et al. (2011), not days as in the right panel. The multiple y-values for given aging times is due to noise in the OH exposure measurement at very low OH exposures corresponding to the first few minutes of the chamber experiment. The caption on the figure has been edited to describe this effect.

Ahern, A. T., Subramanian, R., Saliba, G., Lipsky, E. M., Donahue, N. M., and Sullivan, R. C.: Effect of secondary organic aerosol coating thickness on the real-time detection and characterization of biomass-burning soot by two particle mass spectrometers, Atmos. Meas. Tech., 9, 6117-6137, https://doi.org/10.5194/amt-9-6117-2016, 2016.

T. B. Onasch, A. Trimborn, E. C. Fortner, J. T. Jayne, G. L. Kok, L. R. Williams, P. Davidovits & D. R. Worsnop (2012) Soot Particle Aerosol Mass Spectrometer: Development, Validation, and Initial Application, Aerosol Science and Technology, 46:7, 804-817, DOI: 10.1080/02786826.2012.663948 Willis, M. D., Lee, A. K. Y., Onasch, T. B., Fortner, E. C.,

Williams, L. R., Lambe, A. T., Worsnop, D. R., and Abbatt, J. P. D.: Collection efficiency of the soot-particle aerosol mass spectrometer (SP-AMS) for internally mixed particulate black carbon, Atmos. Meas. Tech., 7, 4507-4516, https://doi.org/10.5194/amt-7-4507-2014, 2014.

Referee #2

Scientific

Referee #2: On p. 4 potential loses in the sampling line are discussed, and a figure is provided in the supplement illustrating the difference between gaseous emissions sampled in the stack directly, to those in the community inlet, binned by saturation concentration. The binned comparison does not suggest a systematic loss in the community inlet either across bins or as a function of volatility. However, there is a significant difference in one of the bins (C* 10^7-10^8). Is this difference well understood (e.g., likely due to a specific class of compounds)? And, how might this difference affect the results and analysis?

Author response: The compounds in this bin do not correspond to a specific class of compounds but to a variety of compounds, including: acetic acid, furfural, furanone, monoterpenes, and methyl glyoxal/acrylic acid (in order of decreasing average abundance across all experiments). The presence of well-known SOA precursors (e.g., monoterpenes) in this volatility bin suggest that it is possible that some SOA precursors are in lower abundance in the mini-chamber relative to the stack. Another possibility is that acetic acid, the most abundant compound in this volatility bin, is preferentially lost during transport to the chamber due to accumulated water on the surfaces of the community inlet. Although preferential loss of some compounds in this volatility bin may affect SOA yields, the observation that total NMOGs correlates well with SOA suggests that some preferential loss of a small subset of compounds would not greatly affect SOA formation.

Referee #2: On p. 7, line 4 the authors state that the dilution factor prior to oxidation influenced observed initial aerosol mass and reference Table 1 in the supplement. It is not clear how the dilution factor is represented in the table. Is it a function of sampling time? This needs a bit more clarification/explanation.

Author response: This text simply refers to the fact that after sampling, experiments are diluted by varying amounts depending on the length of time between sampling and initiation of oxidation (254 nm UV lights). The sentence has been reworded for clarity (page 7, line 8-9):

"The total, initial aerosol mass in the chamber varied widely from experiment to experiment (SI Table 1), averaging 130 ± 103 μg m^{-3} (mean ± 1σ), depending on the amount of fuel burned, fuel type, sampling time, and dilution prior to oxidation."

Referee #2: The relationship between reported enhancement ratios in this work with previously published ratios is discussed on p. 7, first paragraph. The authors suggest that once aging and collection efficiency are taken into account, the results are broadly consistent with other results, and not overestimates. However, based on Fig. S6 panel b, where OA enhancement ratios are plotted as a function of aging time, the reported enhancements are still a factor of 2+ higher than Ortega et al. Are the Lim et al. enhancement ratios in the right panel actually for CE =1? They seem significantly higher than what is presented in the left panel (and it is assumed that both are for CE = 1). In addition, the average appears to be ~3, which is the CE corrected-value reported in the main text.

Author response: We thank the reviewer for pointing this out; Fig. S6b was mistakenly showing the CE corrected data instead of CE = 1. The figure has been updated so that both panels show CE = 1; however, even after correcting the figure, OA enhancements measured in the mini-chamber are significantly higher than those seen in Ortega et al. (2013). The text in the manuscript has been changed to reflect this (page 7, lines 18-23):

"The average OA enhancement ratio was 3.5 ± 1.7. This is considerably higher than reported in previous studies (Ahern et al., 2019; Hennigan et al., 2011; Ortega et al., 2016; Tkacik et al., 2017), but once differences in OH exposure (as well as AMS CE) are taken into account, these results are broadly consistent with previous chamber studies and only somewhat higher than previous flow tube experiments (Fig. S6)."

Referee #2: In the discussion of correlation of measured SOA formation with different parameters (pp. 8-9), it is suggested that the reasonable correlations exist between SOA and total NMOG, with some relationship to POA, and when corrected for aging time. On p. 9, line 2, the authors state that the NMOG correlated well with POA (not shown), and thus POA is also well correlated with SOA. The correlation with POA, at least based on r2 values, actually appears to be better than the correlation with total NMOG. If the goal is a simplified parameterization, why not just use POA?

Author response: While we provide a simple SOA parameterization based on NMOG (i.e., carbon yield from biomass burning emission), the goal of the paper is a more mechanistic understanding of the underlying chemistry and gas-phase precursors. As such, we present the NMOG parameterization in the manuscript, but also provide the relationships between SOA and POA Fig. S9 for purposes where POA measurements may be more readily available. The following text was added to the main text (page 9, lines 12-14):

"As the goal of this work is to provide a more mechanistic understanding of the underlying chemistry, relationships between SOA and NMOGs are shown in the main text; relationships between POA and SOA are given in Fig. S9 for purposes where POA measurements may be more readily available."

Referee #2: In the discussion of the results presented in Figs. 4 and 5, it is suggested that the relative insensitivity of SOA to NMOG m/z cutoff below ~m/z 135 is either due to the contribution of higher volatility/lower molecular weight species, or other compounds which are not measured by the PTRMS, but correlated with these smaller NMOG molecules. It seems like there may be sufficient data available to look at the ratio of likely SOA precursors to total NMOG to test this hypothesis. Also, while it is not discussed, to the observed carbon yields themselves lend some insight to the likely precursors?

Author response: We appreciate this suggestion. We have looked in more detail at the precursors and their relationships (or lack thereof) with SOA formation. We were not able to determine specific precursors or a specific class of compounds that show significantly stronger correlations with SOA than the total NMOG loading. Monoterpenes, low/high temperature factors, each m/z cutoff, and compounds binned by carbon number or volatility did not show improved correlations with SOA compared to total NMOG loadings. In addition, we also examined the correlation between SOA and the top SOA precursors identified in Bruns et al. (2016), including benzene, phenol, naphthalene, and related compounds and they do not show good correlations SOA formation. These compounds have are now explicitly mentioned in the main text (page 9, line 30).

Editorial

Referee #2: p. 8, line 20: Recommend changing "common SOA precursors" to "monoterpenes", since that is the only precursors show in S.7.

Author response: Text changed to "monoterpenes."

Referee #2: p.9, line 23: It would be interesting to see the correlation plots of the two different temperature NMOG factors with SOA. Could these be added to the supplement?

Author response: SOA (carbon mass) correlation plots for low and high temperature combustion factors have been added to the supplement (Fig. S10). High and low temperature factors for each burn are calculated by calculating the fraction high/low factor for the initial NMOG composition (before oxidation) and multiplying by the total NMOG loading (ppb C). Reference to SI added to the main text (page 9, line 34 – page 10, line 2):

"Correlations between NMOGs and SOA when splitting total NMOGs by factor type are weak (Fig. S10), indicating that both factors contain compounds that contribute to SOA formation."

Secondary organic aerosol formation from the laboratory oxidation of biomass burning emissions

Christopher Y. Lim[1a], David H. Hagan[1], Christopher D. Cappa[2], Matthew M. Coggon[3,4], Abigail R. Koss[3,4,5,b], Kanako Sekimoto[3,4,6], Joost de Gouw[1,2,3], Carsten Warneke[3,4], Jesse H. Kroll[1]

[1]Department of Civil and Environmental Engineering, Massachusetts Institute of Technology, Cambridge, MA 02139, USA
[2]Department of Civil and Environmental Engineering, University of California, Davis, CA 95616, USA
[3]Cooperative Institute for Research in Environmental Sciences, University of Colorado, Boulder, CO 80309, USA
[4]NOAA Earth System Research Laboratory, Chemical Sciences Division, Boulder, CO 80305, USA
[5]Department of Chemistry, University of Colorado, Boulder, CO 80309, USA
[6]Department of Civil and Environmental Engineering, University of California, Davis, CA 95616, USA
[a]now at Department of Chemistry, University of Toronto, Toronto, ON M5S 3H4, Canada
[b]now at TOFWERK USA, Boulder, CO 80301, USA

Correspondence to: Jesse H. Kroll (jhkroll@mit.edu), Christopher Y. Lim (cy.lim@utoronto.ca)

Abstract. Biomass burning is an important source of aerosol and trace gases to the atmosphere, but how these emissions change chemically during their lifetimes is not fully understood. As part of the Fire Influence on Regional and Global Environments Experiment (FIREX 2016), we investigated the effect of photochemical aging on biomass burning organic aerosol (BBOA), with a focus on fuels from the western United States. Emissions were sampled into a small (150 L) environmental chamber and photochemically aged via the addition of ozone and irradiation by 254 nm light. While some fraction of species undergoes photolysis, the vast majority of aging occurs via reaction with OH radicals, with total OH exposures corresponding to the equivalent of up to 10 days of atmospheric oxidation. For all fuels burned, large and rapid changes are seen in the ensemble chemical composition of BBOA, as measured by an aerosol mass spectrometer (AMS). Secondary organic aerosol (SOA) formation is seen for all aging experiments and continues to grow with increasing OH exposure, but the magnitude of the SOA formation is highly variable between experiments. This variability can be explained well by a combination of differences in OH exposure and the total concentration of non-methane organic gases (NMOGs) in the chamber before oxidation, as measured by PTR-ToF-MS (r^2 values from 0.64 to 0.83). From this relationship, we calculate the fraction of carbon from biomass burning NMOGs that is converted to SOA as a function of equivalent atmospheric aging time, with carbon yields ranging from 24 ± 4 % after 6 hours to 56 ± 9 % after 4 days.

1 Introduction

Biomass burning is a major source of particulate matter and trace gases to the atmosphere, and strongly affects global air quality and climate (Akagi et al., 2011; Bond et al., 2004; Liu et al., 2017). In fire-prone regions such as the western United States, the frequency and intensity of wildfires have increased over the past several decades, due to fire management practices and climate change (Westerling et al., 2006), and this trend is expected to continue in the coming decades (Dennison et al.,

Deleted: Lim[1]
Deleted: [a]
Deleted: Civil and Environmental Engineering, Massachusetts Institute of Technology, Cambridge, MA 02139, USA
Deleted: experiment-to-experiment

2014; Spracklen et al., 2009). Emissions from fires have been the subject of intense study, but primary emissions alone do not determine the atmospheric impacts of biomass burning, since smoke plumes can be transported thousands of kilometers and undergo dramatic chemical changes over their lifetimes in the atmosphere (Andreae et al., 1988; Cubison et al., 2011). In particular, biomass burning organic aerosol (BBOA) is subject to atmospheric aging processes that could significantly alter the climate- and health-relevant properties of biomass burning emissions (Hennigan et al., 2012; Vakkari et al., 2014). Such processes include oxidation of gas-phase compounds followed by partitioning to the particle phase, forming secondary organic aerosol (SOA); direct oxidation of molecules in the particle phase through heterogeneous reactions; and evaporation of particulate semi-volatile molecules upon plume dilution, potentially followed by subsequent gas-phase oxidation. However, despite the potential importance of aging on biomass burning emissions, the effect of aging on BBOA composition and loading over multiday timescales is not well-constrained, and usually is not included in global chemical transport models (Shrivastava et al., 2017).

Field measurements provide strong evidence that the composition of BBOA changes significantly when photochemically aged. In aircraft measurements of biomass burning plumes, OA consistently becomes more oxidized downwind, relative to the source of emissions (Capes et al., 2008; Cubison et al., 2011; Forrister et al., 2015; Jolleys et al., 2015; Jolleys et al., 2012). Additionally, decreases in reactive tracers from biomass burning, such as levoglucosan, are observed after aging when compared to their contribution to fresh emissions (Cubison et al., 2011). Despite these consistencies, field measurements show mixed results with regards to whether or not there is an increase in net SOA downwind of fires. Net SOA formation is usually characterized by an OA enhancement ratio, defined as the ratio between fresh and aged $\Delta OA/\Delta CO$ measurements to account for plume dilution. Some studies show that little to no net secondary organic aerosol is formed over the course of several days of aging, or even that a loss of organic mass can occur (Akagi et al., 2012; Capes et al., 2008; Cubison et al., 2011; Hecobian et al., 2011; Jolleys et al., 2015; Jolleys et al., 2012; May et al., 2015). However, other studies show that significant OA enhancement can occur as well (DeCarlo et al., 2010; Vakkari et al., 2018; Yokelson et al., 2009).

Laboratory studies intended to constrain the effects of aging on biomass burning emissions have also had variable results. Consistent with field measurements, laboratory experiments in which emissions from open burning and wood stoves were photochemically aged found that BBOA became increasingly oxidized and tracers were depleted with increased aging time (Ahern et al., 2019; Bertrand et al., 2018; Cubison et al., 2011; Grieshop et al., 2009; Hennigan et al., 2011; Ortega et al., 2013; Tkacik et al., 2017). Most laboratory experiments investigating the aging of biomass burning emissions find that significant amounts of SOA are formed in most, but not all, cases (Ahern et al., 2019; Bruns et al., 2016; Grieshop et al., 2009; Hennigan et al., 2011; Ortega et al., 2013; Tiitta et al., 2016; Tkacik et al., 2017). Even under constrained laboratory experimental conditions, these studies show significant variability in SOA formation between burns of similar or even identical fuels. This variability is often attributed to differences in burning conditions (e.g., flaming and smoldering) (Hennigan et al., 2011) or the presence of unmeasured SOA precursors (Bruns et al., 2016; Grieshop et al., 2009; Ortega et al., 2013), but predicting biomass

burning SOA across fuel types and burning conditions has remained a challenge. Very recently, Ahern et al. (2019) showed that the detailed characterization of the hundreds of compounds emitted from a given burn, coupled with estimated SOA yields from each, enables the prediction of SOA formation to within roughly a factor of two. This approach establishes a clear link between the gas-phase emissions and SOA formation, but relies critically on a comprehensive understanding of emission profiles, which may exhibit substantial burn-to-burn variability.

The high degree of variability in net OA observed from biomass burning studies leads to a large range of estimates of SOA from biomass burning, which span nearly two orders of magnitude (Shrivastava et al., 2017). The range of global estimates is thus essentially unconstrained, with some studies ranking biomass burning as an insignificant source of SOA and others ranking it as the major source of global SOA (Shrivastava et al., 2015, 2017). Understanding the evolution of biomass burning emissions is necessary to better evaluate the effects of biomass burning on air quality, human health, and climate. To this end, we describe the results from a set of laboratory aging experiments on a variety of fuels, employing an oxidation reactor coupled with real-time measurements of the composition of both the particle-phase and gas-phase emissions, to better constrain the effects of aging on biomass burning emissions.

2 Methods

2.1 Experimental setup and emissions sampling

Experiments were carried out as part of the Fire Influence on Regional and Global Environments Experiment (FIREX 2016) at the USDA Fire Sciences Laboratory (FSL) in Missoula, MT, with the goal of better understanding the evolution of biomass burning emissions within a controlled environment. Experiments took place during the "stack burn" portion of FIREX, in which fuels were burned beneath a 1.6 m diameter, 17 m tall exhaust stack, and were well mixed before being characterized at the top of the stack. Fuels burned were characteristic of the western U.S. and included Engelmann spruce, lodgepole pine, subalpine fir, chamise, manzanita, Douglas fir, ponderosa pine, and sagebrush (Selimovic et al., 2018). For each of these fuels, components of each fuel (e.g., canopy, litter, duff) were burned individually, to determine differences between components, and in combination, as they would in natural wildfires and prescribed burns. In addition to these fuels, several other fuel types were included, such as peat, dung, Excelsior (wood shavings), rice straw, loblolly pine, and bear grass. The weight of fuel used for each experiment was between 250–6000 g. Details of each burn sampled are given in the Supporting Information (SI Table 1); here we focus on results from 20 burns (out of 56 sampled total), for which aging experiments were carried out, the full analytical instrument suite (described in Sect. 2.2) collected data, and particle wall-loss rates were unaffected by UV irradiation (also discussed in Sect. 2.2).

Aging experiments were conducted in a 150 L PFA environmental chamber (the "mini-chamber"), an oxidation reactor of intermediate size between commonly-used oxidation flow reactors (with volumes of < 15 L) and large environmental chambers

Deleted:

Commented [CL1]: corrected

(> 1000 L). The mini-chamber was located in the wind tunnel room in the FSL; smoke from the top of the stack was transported to the wind-tunnel room with a 30 m long community inlet (see Fig. S1). In order to minimize interactions of the smoke with the walls of the inlet, the tubing had a large diameter (8 in. diameter aluminum ducting) and fast flow (inline fan at the ducting exhaust pulling at 700 cfm, giving a transport time of < 2 s). Smoke from the community inlet was sub-sampled from the center of the flow using an ejector diluter pressurized with clean air, then passed through 1 m of passivated stainless-steel tubing and a PM_1 cyclone, and injected into the chamber. Comparisons of fresh emissions between direct measurements from the top of the stack and measurements in the mini-chamber indicated some loss of gases and particles along the community inlet and transfer line, but these were relatively minor (< 8 % per volatility bin on average) and while they might affect SOA yields somewhat, are not expected to affect the overall results significantly (Fig. S2).

Prior to sampling, the chamber was flushed with clean air from a zero-air generator (Teledyne 701H) and humidified air (total 15 slpm) for approximately 45 minutes, leading to background particle concentrations 10^3–10^4 times smaller than the peak concentrations during filling. Relative humidity remained in the range of 25–40 % throughout the entire experiment. Emissions sampling was initiated at the beginning of the burn and continued until the fuel was completely burned or the chamber particle concentration notably declined from its maximum concentration. Sampling generally lasted for a significant fraction of each fire (5–20 minutes sampling time, while fires burned for 5–40 minutes) and initial concentrations of species within the chamber were diluted by a factor of ~7 relative to concentrations in the stack. Once sampling was stopped, the chamber was allowed to mix passively for 5–10 minutes while the fresh emissions were characterized. The chamber was operated in semi-batch mode, meaning that after sampling, the chamber was continuously diluted with clean air while the smoke was oxidized and monitored. Chemical aging was initiated by OH, generated from both ozone photolysis and reaction of the resulting $O(^1D)$ with water vapor and the photolysis of other OH precursors present in the smoke (e.g., HONO). A mercury pen-ray lamp (Jelight Model 600 ozone generator) was used to generate ozone (50–100 ppb in dilution air), which was added to the chamber starting just after the sampling period and continually added over the course of the experiment. The O_3 concentration in the chamber was typically lower at the start of each experiment and higher toward the end, and ranged from 10–80 ppb throughout. OH oxidation was initiated by exposing the chamber to 254 nm UV light (one UVP, LLC. XX-40S bulb, for a chamber averaged photon flux of ~3 x 10^{15} photons cm^{-2} s^{-1}). Use of low-wavelength UV light can introduce non-OH chemistry (Peng et al., 2016); however, loss rates of common compounds from biomass burning such as toluene, phenol, and naphthalene agree well with predicted loss rates from OH reaction alone (average [OH] ≈ 2 x 10^8 molec cm^{-3}), indicating that for these compounds UV photolysis is negligible. However, photolysis can be competitive with OH reactions for compounds that undergo rapid photolytic degradation at 254 nm. Such species, which are characterized by a low ratio between their OH reaction rate constant to absorption cross section (k_{OH} / σ_{254nm} < 1.5 x 10^7 cm/s), and high quantum yields, include conjugated carbonyls (e.g., furfural, benzaldehyde) (Coggon et al., 2019). These species will therefore undergo substantially more photolysis in the present experiments compared to atmospheric conditions; however, for the vast majority of compounds studied here, the dominant reactive loss (as in the atmosphere) is by reaction with OH (Coggon et al., 2019). Oxidation lasted 30–60 minutes, then the

Deleted: dilution factors

Deleted: approximately 7 times

chamber was flushed with clean air before the next experiment. At the end of each day, the chamber was left to flush with clean air and with four UV lamps on overnight. Seeded blanks (with ammonium sulfate particles) were run and showed negligible OA formation indicating that the cleaning procedure was successful. In addition to the aging experiments, control runs were conducted without UV light and used to characterize the evolution of the smoke in the absence of OH oxidation.

Particles and gases exiting the reactor were monitored with a suite of analytical instruments. Particle composition measurements were made with an aerosol mass spectrometer with a standard tungsten vaporizer (AMS, Aerodyne Research, Inc.) which measures the mass and composition of non-refractory particles with diameters between 70 nm and 1 μm (DeCarlo et al., 2006). Black carbon mass was measured with a Single Particle Soot Photometer (SP2, Droplet Measurement Technologies) and SP-AMS (Aerodyne Research Inc., Onasch et al., (2012)). Particle size distributions were measured with a Scanning Electrical Mobility Spectrometer (SEMS, Brechtel). All particle-phase measurements were made alternating between a two-stage thermal denuder (150 °C and 250 °C) and a room-temperature bypass line. From these measurements, particle organic mass fraction remaining (MFR) was calculated by comparing the thermally denuded particle organic mass to the mass after the bypass line. Non-methane organic gases (NMOGs) were measured with a proton-transfer-reaction time-of-flight mass spectrometer (NOAA PTR-ToF-MS); these measurements are described in detail elsewhere (Koss et al., 2018, Sekimoto et al., 2018), and the oxidation chemistry of NMOGs is described in a companion paper (Coggon et al., 2019). Auxiliary measurements of inorganic gases included O_3 (2B Technologies, Model 202), CO (Teledyne, Model T300), and CO_2 (LI-COR, LI-840A). Particle optical properties were monitored with a three-wavelength photoacoustic spectrometer (PASS-3), a two-wavelength cavity ring down photoacoustic spectrometer (CRD-PAS), and a cavity attenuated phase shift spectrometer (CAPS). Optical measurements from these instruments are not used in the present study, and instead will be discussed in a future publication (Cappa et al., in preparation).

Deleted: instrumentation

2.2 Data analysis

Particle mass and composition data from the AMS were analyzed using the ToF-AMS analysis toolkits (Squirrel version 1.57I, Pika version 1.16I) using the "improved-ambient" method for calculating oxygen-to-carbon (O/C) and hydrogen-to-carbon (H/C) elemental ratios (Canagaratna et al., 2015). Mass concentrations must be corrected for changes in AMS collection efficiency (CE), as well as wall loss and dilution. This is often done in chamber experiments by normalizing measured SOA mass concentrations to that of an inert internal tracer. However, we were unable to find a suitable tracer in these experiments: sulfate changes as a result of oxidation of emitted SO_2, black carbon (when present in high concentrations) exhibited wall losses different from OA (as described below) and appeared not to be homogeneously mixed with the OA (McClure et al., in prep), and POA tracers (such as the $C_7H_{11}^+$ ion, recently used by Ahern et al. (2019)) are likely to be lost via heterogeneous oxidation at the high OH exposures examined here. Thus, corrections for CE, dilution, and particle wall loss were carried out individually, as described below.

CE and particle density were calculated by comparing AMS particle time-of-flight (PToF) and SEMS size distributions (Bahreini et al., 2005) .This could only be done for the subset of data points with PToF and SEMS distributions that could be fit to lognormal functions, did not show significant particle nucleation, and had low rBC concentration (see below). An AMS CE correction was then applied to the entire data set by parameterizing the exponential relationship between AMS CE with the particle MFR (Fig. S3). Over longer timescales, when dilution is more significant and OA concentrations are lower, such OS_C changes are likely to reflect the oxidation of longer-lived gases.This indicates that particles are becoming less volatile and more likely to be (semi-)solid, and therefore likely to have a lower CE due to increased bounce off of the AMS vaporizer (Matthew et al., 2008; Virtanen et al., 2010). Calculated AMS collection efficiencies range from 0.35 to 0.64, with the average CE of fresh emissions equal to 0.54 and average CE of aged (i.e., end-of-oxidation) emissions equal to 0.40. We note that this CE value of 0.54 for fresh emissions is substantially lower than the value of 1 typically assumed in such experiments (Ahern et al., 2019; Hennigan et al., 2011; Heringa et al., 2011; Ortega et al., 2013; Tkacik et al., 2017).

Commented [CL2]: Refs added

Acetonitrile, an inert tracer species (k_{OH} = 2.16 x 10^{-14} cm^3 $molec^{-1}$ s^{-1}) (Atkinson et al., 2001), was used to correct all data for chamber dilution. An exponential function was fitted to the decay of acetonitrile for each experiment ($\tau_{dilution}$ ~ 20 minutes). All gas- and particle-phase species concentrations are corrected for dilution using an experiment-specific dilution rate. Dilution rates calculated from the fitted decay of acetonitrile agree well with estimates based on chamber volume and flow rates; this is in contrast with dilution rates derived from CO, which is produced in the chamber during oxidation. Particle mass concentrations were also corrected for loss to the chamber walls, by fitting an exponential equation to the particle organic mass concentration during a control experiment in which the UV lamps were not turned on (τ_{wall} = 35 min; Fig. S4). Comparison of wall loss rates calculated between two dark experiments and size-dependent wall loss rates calculated from SEMS data yield similar results. Fires with the lowest initial AMS OA to SP-AMS BC ratios (OA/rBC < 3.4) showed enhanced wall loss rates upon UV irradiation, likely due to photoionization of BC or polycyclic aromatic hydrocarbons present on the particle surface (Burtscher, 1992; Mohr et al., 1996), followed by increased electrostatic interactions with the chamber walls. This complicates the wall loss correction, and such low OA/rBC burns are excluded from this analysis (see SI Table 1). All particle concentrations presented, unless otherwise noted, are corrected for collection efficiency, dilution, and wall loss. Gases were corrected for dilution only; control runs showed that wall loss was not a major loss pathway for most primary intermediate volatility organic compounds (IVOCs; Fig. S5).

OH exposures in the chamber were estimated by measuring the decay of an OH tracer, deuterated *n*-butanol (D9, 98%, Cambridge Isotope Laboratories), added at the beginning of each experiment (10 µL, 2% in water). OH exposure was then calculated from the dilution-corrected concentration of deuterated butanol and its reaction rate coefficient with OH (k = 3.4 x 10^{-12} cm^3 $molec^{-1}$ s^{-1}) (Barmet et al., 2012). Differences in the initial concentration of OH precursors (e.g., O_3 and HONO) in the chamber, OH sinks, and experiment duration resulted in variations in total OH exposure from experiment to experiment, with end-of-experiment OH exposures (calculated at the point when UV lamps are turned off) ranging from 1–10 days of

atmospheric aging. Throughout this work, OH exposure is converted to equivalent atmospheric aging time (in days) by assuming an average OH concentration of 1.5 x 10^6 molec cm^{-3}.

3 Results and discussion

3.1 Loading and composition of fresh and aged biomass burning particles

The total, initial aerosol mass in the chamber varied widely from experiment to experiment (SI Table 1), averaging 130 ± 103 μg m^{-3} (mean ± 1σ), depending on the amount of fuel burned, fuel type, sampling time, and dilution prior to oxidation. For all experiments considered here, the organic fraction dominated the composition of the primary particle mass (as measured by the sum total of the AMS and SP2, with initial primary OA (POA) concentrations accounting for 70–99 % of the total aerosol mass. The initial fraction of black carbon (BC) mass also varied significantly (0–30 % of total aerosol mass) and was highly dependent on fuel type, with the highest BC mass fractions observed for chaparral and Excelsior fuels. Concentrations of non-BC inorganic components (AMS measured nitrate, sulfate, ammonium, and chloride) were variable, but low for all experiments (≤ 8 % of total aerosol mass). After initiation of oxidation, organic aerosol loadings grew substantially for all experiments (Fig. 1a). The average mass loading of SOA formed (corrected OA mass at the end of the experiment, minus the OA mass prior to OH oxidation) was 260 ± 250 μg m^{-3}. Alternatively, the amount of SOA at the end of experiment can be expressed as an OA enhancement ratio, defined as the final OA mass (secondary + primary) divided by the initial (primary) OA mass. The average OA enhancement ratio was 3.5 ± 1.7. This is considerably higher than reported in previous studies (Ahern et al., 2019; Hennigan et al., 2011; Ortega et al., 2016; Tkacik et al., 2017), but once differences in OH exposure (as well as AMS CE) are taken into account, these results are broadly consistent with previous chamber studies and only somewhat higher than previous flow tube experiments (Fig. S6). Discussion of the relationship between SOA formation and gas phase composition will be discussed further in Sect. 3.2.

Commented [CL3]: Edited

Commented [CL4]: Edited

The chemical composition of the primary organic particulate matter varied substantially between experiments. The initial O/C ranged from 0.20 to 0.60 (0.35 ± 0.09) and initial H/C ranged from 1.72 to 1.85 (1.77 ± 0.04), indicating significant variation in POA elemental composition. Elemental ratios stayed constant in the chamber for each given experiment until the lights were turned on. Similarly, control experiments (with no oxidation) showed constant OA/BC, O/C, and H/C over the course of the run, indicating that OA mass and overall oxidation state of biomass burning POA is stable in the chamber without exposure to UV light, despite the potential for semi-volatile compounds to partition to the gas phase and/or be lost to the chamber walls (Ahern et al., 2019; Grieshop et al., 2009; Hennigan et al., 2011; May et al., 2013).

Deleted: significantly

OH oxidation, initiated in the chamber by exposure to UV light, rapidly changes the composition of OA, as shown in Fig. 1b–d. Gas-phase chemistry in the mini-chamber is discussed in detail in a companion publication (Coggon et al., 2019). Despite differences in initial composition between experiments, OA in all experiments undergoes a large increase in O/C and decrease

Deleted: will be

Deleted: forthcoming

in H/C (Fig. 1b), and a corresponding increase in average carbon oxidation state (OS_C, equal to 2 O/C – H/C) (Fig. 1c). OS_C for all fuels increases with increasing OH exposure, with an average, end-of-experiment increase in OS_C of 1.33 ± 0.50. Most of this change occurs during the initial period of oxidation (equivalent timescales of just 1–2 days); after this, changes in OS_C still occur, but over much longer timescales. Over longer timescales, when dilution is more significant and OA concentrations are lower, such OS_C changes are likely to reflect the oxidation of longer-lived gases. Both condensation of SOA and heterogeneous oxidation (direct reactions between gas-phase oxidants and particle-phase organic molecules) can contribute to the observed increases in oxidation state. However, the initial rate of change for aging of biomass burning emissions (gases and particles combined) is much faster than the average rate of OS_C change measured in laboratory heterogeneous OH-oxidation experiments (Kroll et al., 2015) (shown as the grey line in Fig. 1c), implying that condensation of highly oxidized secondary mass is the main driver for the changes in composition observed.

Similar to the elemental ratios, the initial fraction of the primary organic signal from the AMS fragment ion $C_2H_4O_2^+$ ($f_{C2H4O2+}$) varies from burn to burn (mean 2.2 ± 1.2 %). This fragment is a small (< 6 %) contributor to the overall OA mass spectrum, but is known to correlate with levoglucosan (and related molecules) and is commonly used as a tracer for biomass burning POA (Cubison et al., 2011). Figure 1d shows the evolution of $f_{C2H4O2+}$, normalized to its value at the start of each experiment. This ion is known to correspond to semi-volatile species (Grieshop et al., 2009), and changes to $f_{C2H4O2+}$ (~ 25 % loss) are observed even in the absence of oxidation; however, oxidation greatly enhances the rate and magnitude of its decrease. Under oxidation conditions, the contribution of this fragment to the total organic mass decreases dramatically over the course of 1–2 days of equivalent OH exposure, then stabilizes after that. This is in agreement with previous aircraft studies, which show that even in highly aged airmasses, a small amount of this tracer remains elevated relative to the atmospheric background level (Cubison et al., 2011), potentially due to contribution of other molecules to this tracer. Overall, the chemical changes observed here are likely dominated by the formation of SOA, although heterogeneous oxidation, dilution-driven evaporation, and wall loss may also contribute.

3.2 Secondary organic aerosol formation

All aging experiments show substantial SOA formation, with OA mass continuing to increase with extended aging time (Fig. 1a). Consistent with previous studies, the correlations between OA mass enhancement ratio and various parameters that could affect SOA production (e.g., OH exposure, POA, monoterpenes, total NMOG concentration) are weak at best (Fig. S7). However, the absolute amount of SOA formed does appear to correlate with some of these. Figure 2 shows the relationship between SOA formed by the end of each experiment (μg m^{-3}) and the initial concentration of total NMOGs in the chamber (ppb) measured by the PTR-ToF-MS. A positive correlation is seen between the two variables, but the correlation is not especially strong (r^2 = 0.51). A confounding variable in this relationship is the difference in total OH exposure between experiments, as shown in the color scale. To account for the differences in OH exposure, Fig. 3 shows the same relationship

between SOA and NMOG concentration, but now compared at equal OH exposures (0.25, 0.5, 1, 2, 3, and 4 days of atmospheric aging) and with both axes converted to carbon concentration. Although there is still significant scatter, possibly due to differences in initial POA levels (Fig. S8), there is an improved correlation (r^2 = 0.64–0.83) between SOA and NMOG carbon mass at each OH exposure. Subplots in Fig. 3 contain different numbers of data points, due to the differences in final OH exposure achieved in each experiment. As such, the r^2 values are not strictly comparable, but are labeled to show the correlation in all cases. Additionally, the slopes of these plots exhibit a clear trend, increasing with OH exposure. This indicates that a greater fraction of carbon from NMOGs is converted to SOA as aging time increases, consistent with continual SOA formation over long aging timescales. Total PTR-ToF-MS measured NMOGs also correlates well with POA concentration; as such, POA shows a similarly strong relationship with SOA. As the goal of this work is to provide a more mechanistic understanding of the underlying chemistry, relationships between SOA and NMOGs are shown in the main text; relationships between POA and SOA are given in Fig. S9 for cases in which POA measurements may be more readily available.

The correlation between SOA formation and the initial chamber concentration of NMOGs is reasonable, since NMOGs provide the carbon that drives SOA growth. However, the PTR-ToF-MS measures many compounds that likely do not contribute to SOA formation (e.g., small compounds such as methanol and acetonitrile). In addition to comparing SOA to the initial NMOG concentration, we can examine how SOA formation correlates with the concentration of NMOGs above some molecular weight cutoff. Figure 4 shows the correlation coefficient for the linear fit between SOA carbon mass and summed NMOG carbon mass at each molecular weight cutoff for 1 day of equivalent aging. While low molecular weight NMOGs are not expected to contribute to SOA mass, the correlation between SOA carbon mass and initial NMOG carbon mass does not improve substantially when these are excluded (left side of Fig. 4). In fact, the correlation between SOA is relatively insensitive to the *m/z* cutoff point, until only compounds with molecular weight greater than monoterpenes (*m/z* > 137) are considered. After this point the correlation drops rapidly to zero, likely because the PTR-ToF-MS signal is very low in this mass range, and/or compounds with 10 or fewer carbon atoms are major contributors to SOA formation (or correlate with some unmeasured SOA-forming species). This suggests that the ratio of SOA precursors to the total concentration of measured NMOGs is relatively constant between experiments. The rapid step change after *m/z* 137 might suggest the importance of monoterpene chemistry to SOA formation, consistent with Ahern et al. (2019); however, we do not observe strong correlations between SOA and monoterpenes alone, nor any other single SOA precursor (e.g., isoprene, benzene, phenol, naphthalene), nor any subset or class of compounds measured by the PTR-ToF-MS (e.g., IVOCs). PTR-ToF-MS measurements taken directly from the FSL exhaust stack show that although the NMOG emissions are incredibly complex, much of the variability in emissions (~85 %) can be described by just two emission factors (derived using positive matrix factorization, or PMF), one high-temperature combustion factor and one low-temperature combustion factor (Sekimoto et al., 2018). Correlations between NMOGs and SOA when splitting total NMOGs by factor type are weak (Fig. S10), indicating that both factors contain compounds that contribute to SOA formation.

Deleted: (Fig. S9).

Deleted: We do not see improved correlations

Commented [CL5]: Edited

Previous biomass burning aging experiments with both aerosol and NMOG measurements have not observed this relationship between SOA and total NMOGs (Ortega et al., 2013) or individual SOA precursors (Bruns et al., 2016; Grieshop et al., 2009; Ortega et al., 2013; Tkacik et al., 2017). Most such studies identified only half or less of the NMOG signal and/or were limited to a small number of experiments (Grieshop et al., 2009; Ortega et al., 2013; Tkacik et al., 2017); this could potentially explain why similar correlations between total VOCs and SOA have not been observed before. By contrast, the use of PTR-ToF-MS in the present study enables the measurement of ~50–80 % of reactive gas-phase carbon from biomass burning, making it a good tool for characterizing the total organic gas-phase emissions from fires (Hatch et al., 2017). In this analysis, we have included both identified and calibrated PTR-ToF-MS ions (~90 % of the signal, approximately 150 ions) as well as an additional 370 unidentified ions (Koss et al., 2018). This is roughly comparable to the number of compounds identified and quantified in recent speciated studies of biomass burning emissions (Hatch et al., 2015), which have been shown to enable reasonable bottom-up estimates of total SOA formation (Ahern et al., 2019). However, such speciated approaches require estimates of SOA yields from each precursor, which might be unknown or highly uncertain. As an alternative approach, the initial total NMOG concentration measured by the PTR-ToF-MS, in conjunction with OH exposure, provides a reasonable predictor for the amount of SOA formation without the need for speciated aerosol yields.

Recent work has pointed to the importance of "non-traditional" SOA precursors to SOA formation for residential wood combustion of a single fuel type (beech wood) (Bruns et al., 2016). These precursors include semivolatile and intermediate-volatility volatile organic compounds (S/IVOCs) such as phenols and naphthalenes (Bruns et al., 2016). However, the majority of gas-phase carbon observed in this study is in compounds with low carbon number ($n_C < 7$), with corresponding volatilities that are weighted towards volatile compounds ($c_0 > 10^7$ μg m^{-3}) rather than S/IVOCs (Fig. 5). This means that SOA from biomass burning is strongly influenced by the oxidation of relatively small, volatile species, and not S/IVOCs, a result consistent with Ahern et al. (2019); alternatively, this could mean that the PTR-ToF-MS does not measure all important SOA precursors, but measures compounds that are co-emitted and correlate well with them.

From each of the relationships between SOA carbon mass and initial NMOG carbon mass (linear fits in Fig. 3), an effective carbon yield can be calculated. Carbon yield is defined here as the SOA formed at a given OH exposure divided by the total NMOG carbon reacted at each respective OH exposure. The amount of gas phase carbon reacted ($\Delta[C]_{NMOG}$) is estimated from the initial concentration of PTR-ToF-MS measured gas-phase organic carbon in the chamber before oxidation, experiment-specific dilution rates, and speciated OH reaction rates for identified compounds present in each fire (Koss et al., 2018). We are not able to directly measure the amount of NMOG reacted, due to the dilution loss of NMOG (gases removed from the chamber before they can be reacted with OH), formation of secondary gas-phase products, and potential off-gassing of non-SOA forming low molecular weight NMOG from the chamber walls, leading to calculated SOA yields greater than unity. Carbon yields as a function of atmospheric age are shown in Fig. 6, and range from 24 ± 4 % at 0.25 days of equivalent

atmospheric oxidation to 56 ± 9 % after 4 days of equivalent atmospheric oxidation. Since the PTR-ToF-MS does not measure the true total NMOG concentration (e.g., not all alkanes and alkenes are measured), these carbon yields are likely to be upper bounds. The calculated yields use our best estimate of OA carbon mass, using the AMS CE correction described previously. The grey points in Fig. 6 show the carbon yields assuming a constant AMS CE equal to 1. In both cases, the amount of SOA formed increases with increasing aging time. Accounting for changes in collection efficiency that occur with aging leads to an approximate factor of 4 increase in yields; previous studies assuming a constant or initial AMS CE equal to 1 may significantly underestimate SOA formation (Ahern et al., 2019; Hennigan et al., 2011; Heringa et al., 2011; Ortega et al., 2013). Better constraints on estimates of AMS collection efficiency are needed for improved estimates of SOA formation from biomass burning. Nonetheless, this carbon yield, combined with laboratory- or field-based estimates of NMOG emissions, provides a means for including SOA formation from biomass burning sources within chemical transport models.

The variability in findings from previous lab and field studies on the effect aging has on net SOA from biomass burning can be potentially explained by the effects of dilution on the evolution of BBOA mass. Some fraction of BBOA is semi-volatile, and dilution (in chambers or ambient smoke plumes) will cause volatile OA components to partition from the particle phase to the gas phase (May et al., 2013). Recent modeling work has shown that even in plumes that show no net SOA formation, significant condensation of secondary organic mass may occur (Bian et al., 2017), but net growth can be low (or even negligible) due to dilution-driven evaporation of OA. In ambient plumes, dilution drives semi-volatile species from the particle to gas phase; although this causes a loss in OA mass, it also serves as a source of SVOCs that can condense back onto particles after oxidation, leading to little to no net change in OA. Related to this point, calculated net OA values are also sensitive to the choice of starting point (i.e., t_0). Initial dilution in chamber experiments may result in substantial POA evaporation, which provide high concentrations of SVOCs that are efficiently converted to SOA upon oxidation. However, some laboratory experiments find a net loss of OA mass during aging (Hennigan et al., 2011; Ortega et al., 2013; Tkacik et al., 2017), which we do not observe in the present experiments. Instead we see SOA formation in all photooxidation studies, and no evaporative loss during dilution-only experiments, results consistent with recent work by Ahern et al. (2019). The reason for this is unclear, but could be due to some combination of differences in dilution and wall losses (gas and particle) in chambers and flow tubes, the method of AMS collection efficiency correction, and experimental conditions leading to different peroxy radical (RO_2) chemistry. Chambers such as the mini-chamber have lower initial dilution factors, but much higher OH concentrations, than large chambers potentially favoring condensation from VOC oxidation over evaporation of particle mass. With the potential preference for condensation over evaporation, this present study may be effectively measuring the potential SOA formation while excluding evaporation from the extensive dilution that occurs in biomass burning plumes; therefore, it is primarily accessing the "chemistry" component of OA evolution (Bian et al., 2017). Thus, the carbon yields shown in Fig. 6 need to be combined with a realistic treatment of BBOA partitioning for effective model inputs to describe BBOA evolution in the atmosphere.

5 Conclusions

We show that the OH-initiated aging of biomass burning emissions leads to significant changes in BBOA composition and loading. These changes are dependent on OH exposure, and are especially large over the first few days after emission. Significant amounts of SOA are formed from all fuels studied here, but SOA formation is highly variable. Despite large differences in fuel type and burning conditions, much of this variability can be explained by differences in the initial total NMOG concentration and OH exposure. Correlations between SOA formation and the concentration of initial measured NMOGs in the chamber at given OH exposures are good, with r^2 values between 0.64 and 0.83, and indicate SOA carbon yields between 24% (after 6 hours of equivalent atmospheric oxidation) to 56% (after 4 days). Given total NMOG measurements from future field campaigns, the calculated SOA carbon yields can be used to estimate gross SOA formation from biomass burning in chemical transport models. However, these estimates would likely need to be used in conjunction with estimates of BBOA evaporation rates to calculate the net effect of aging on OA concentrations. Future work investigating the evolution of biomass burning emissions should attempt to further constrain the rates of BBOA evaporation and compare the relative rates of oxidation and dilution from field and laboratory studies. In addition to this, laboratory studies on a wider range of fuels (i.e., those found in areas other than the western U.S.), and under a wider range of reaction conditions (i.e., different RO_2 reaction pathways), will help improve the ability to predict the loadings, properties, and impacts of biomass burning emissions globally.

Deleted: exhibit

Data availability

Data are available from the CSD NOAA archive at:
https://esrl.noaa.gov/csd/groups/csd7/measurements/2016firex/FireLab/DataDownload/ (NOAA, 2019)

Author contribution

Data were interpreted and manuscript was written by CYL and JHK. Mini-chamber construction and operation were by CYL, DHH, and CDC. AMS was operated and data were analyzed by CYL. PTR-ToF-MS was operated and data were analyzed by MMC, ARK, and KS. Experiments were conceived by JHK, CDC, and CW. All co-authors provided manuscript feedback and comments.

Acknowledgments

This work was supported by NOAA AC4 award NA16OAR4310112. CYL and ARK were supported by the NSF graduate research fellowship program. The authors would like to thank Colette Heald for helpful comments, and Edward Fortner, Timothy Onasch, Berk Knighton, Robert Yokelson, the entire of the FIREX science team, and Missoula Fire Sciences Lab staff for support during the project.

References

Ahern, A. T., Robinson, E. S., Tkacik, D. S., Saleh, R., Hatch, L. E., Barsanti, K. C., et al. (2019). Production of Secondary Organic Aerosol During Aging of Biomass Burning Smoke From Fresh Fuels and Its Relationship to VOC Precursors. *Journal of Geophysical Research: Atmospheres*, 2018JD029068. https://doi.org/10.1029/2018JD029068

Akagi, S. K., Yokelson, R. J., Wiedinmyer, C., Alvarado, M. J., Reid, J. S., Karl, T., et al. (2011). Emission factors for open and domestic biomass burning for use in atmospheric models. *Atmospheric Chemistry and Physics*, *11*(9), 4039–4072. https://doi.org/10.5194/acp-11-4039-2011

Akagi, S. K., Craven, J. S., Taylor, J. W., McMeeking, G. R., Yokelson, R. J., Burling, I. R., et al. (2012). Evolution of trace gases and particles emitted by a chaparral fire in California. *Atmospheric Chemistry and Physics*, *12*(3), 1397–1421. https://doi.org/10.5194/acp-12-1397-2012

Andreae, M. O., Browell, E. V., Garstang, M., Gregory, G. L., Harriss, R. C., Hill, G. F., et al. (1988). Biomass-burning emissions and associated haze layers over Amazonia. *Journal of Geophysical Research*, *93*(D2), 1509–1527. https://doi.org/10.1029/JD093iD02p01509

Atkinson, R., Baulch, D. L., Cox, R. A., Hampson Jr., R. F., Kerr, J. A., Rossi, M. J., & Troe, J. (2001). Summary of evaluated kinetic and photochemical data for atmospheric chemistry. *IUPAC Subcommittee on Gas Kinetic Data Evaluation for Atmospheric Chemistry*, 1–56.

Bahreini, R., Keywood, M. D., Ng, N. L., Varutbangkul, V., Gao, S., Flagan, R. C., et al. (2005). Measurements of secondary organic aerosol from oxidation of cycloalkenes, terpenes, and m-xylene using an aerodyne aerosol mass spectrometer. *Environmental Science and Technology*, *39*(15), 5674–5688. https://doi.org/10.1021/es048061a

Barmet, P., Dommen, J., DeCarlo, P. F., Tritscher, T., Praplan, A. P., Platt, S. M., et al. (2012). OH clock determination by proton transfer reaction mass spectrometry at an environmental chamber. *Atmospheric Measurement Techniques*, *5*(3), 647–656. https://doi.org/10.5194/amt-5-647-2012

Bertrand, A., Stefenelli, G., Jen, C. N., Pieber, S. M., Bruns, E. A., Ni, H., et al. (2018). Evolution of the chemical fingerprint of biomass burning organic aerosol during aging. *Atmospheric Chemistry and Physics*, *18*(10), 7607–7624. https://doi.org/10.5194/acp-18-7607-2018

Bian, Q., Jathar, S. H., Kodros, J. K., Barsanti, K. C., Hatch, L. E., May, A. A., et al. (2017). Secondary organic aerosol formation in biomass-burning plumes: Theoretical analysis of lab studies and ambient plumes. *Atmospheric Chemistry and Physics*, *17*(8), 5459–5475. https://doi.org/10.5194/acp-17-5459-2017

Bond, T. C., Streets, D. G., Yarber, K. F., Nelson, S. M., Woo, J. H., & Klimont, Z. (2004). A technology-based global inventory of black and organic carbon emissions from combustion. *Journal of Geophysical Research: Atmospheres*, *109*(14), 1–43. https://doi.org/10.1029/2003JD003697

Bruns, E. A., El Haddad, I., Slowik, J. G., Kilic, D., Klein, F., Baltensperger, U., & Prévôt, A. S. H. (2016). Identification of significant precursor gases of secondary organic aerosols from residential wood combustion. *Scientific Reports*, *6*(May),

1–9. https://doi.org/10.1038/srep27881

Burtscher, H. (1992). Measurement and characteristics of combustion aerosols with special consideration of photoelectric charging and charging by flame ions. *Journal of Aerosol Science*, *23*(6), 549–595. https://doi.org/10.1016/0021-8502(92)90026-R

Canagaratna, M. R., Jimenez, J. L., Kroll, J. H., Chen, Q., Kessler, S. H., Massoli, P., et al. (2015). Elemental ratio measurements of organic compounds using aerosol mass spectrometry: characterization, improved calibration, and implications. *Atmospheric Chemistry and Physics*, *15*(1), 253–272. https://doi.org/10.5194/acp-15-253-2015

Capes, G., Johnson, B., McFiggans, G., Williams, P. I., Haywood, J., & Coe, H. (2008). Aging of biomass burning aerosols over West Africa: Aircraft measurements of chemical composition, microphysical properties, and emission ratios. *Journal of Geophysical Research Atmospheres*, *113*(23), 1–13. https://doi.org/10.1029/2008JD009845

Coggon, M. M., Lim, C. Y., Koss, A. R., Sekimoto, K., Yuan, B., Gilman, J. B., et al. (2019). OH-chemistry of non-methane organic gases (NMOG) emitted from laboratory and ambient biomass burning smoke : evaluating the influence of furans and oxygenated aromatics on ozone and secondary NMOG formation ., (June), 1–42.

Cubison, M. J., Ortega, A. M., Hayes, P. L., Farmer, D. K., Day, D., Lechner, M. J., et al. (2011). Effects of aging on organic aerosol from open biomass burning smoke in aircraft and laboratory studies. *Atmospheric Chemistry and Physics*, *11*(23), 12049–12064. https://doi.org/10.5194/acp-11-12049-2011

Decarlo, P. F., Ulbrich, I. M., Crounse, J., De Foy, B., Dunlea, E. J., Aiken, A. C., et al. (2010). Investigation of the sources and processing of organic aerosol over the Central Mexican Plateau from aircraft measurements during MILAGRO. *Atmospheric Chemistry and Physics*, *10*(12), 5257–5280. https://doi.org/10.5194/acp-10-5257-2010

DeCarlo, P. F., Kimmel, J. R., Trimborn, A., Northway, M. J., Jayne, J. T., Aiken, A. C., et al. (2006). Field-Deployable, High-Resolution, Time-of-Flight Aerosol Mass Spectrometer. *Analytical Chemistry*, *78*(24), 8281–8289. https://doi.org/10.1021/ac061249n

Dennison, P. E., Brewer, S. C., Arnold, J. D., & Moritz, M. a. (2014). Large wildfire trends in the western United States, 1984-2011. *Geophysical Research Letters*, *41*(8), 2928–2933. https://doi.org/10.1002/2014GL059576

Forrister, H., Liu, J., Scheuer, E., Dibb, J., Ziemba, L., Thornhill, K. L., et al. (2015). Evolution of brown carbon in wildfire plumes. *Geophysical Research Letters*, *42*(11), 4623–4630. https://doi.org/10.1002/2015GL063897

Grieshop, A. P., Logue, J. M., Donahue, N. M., & Robinson, A. L. (2009). Laboratory investigation of photochemical oxidation of organic aerosol from wood fires 1: Measurement and simulation of organic aerosol evolution. *Atmospheric Chemistry and Physics*, *9*(4), 1263–1277. https://doi.org/10.5194/acp-9-1263-2009

Grieshop, Andrew P, Donahue, N. M., & Robinson, A. L. (2009). Laboratory investigation of photochemical oxidation of organic aerosol from wood fires 2: analysis of aerosol mass spectrometer data. *Atmospheric Chemistry and Physics*, *9*, 2227–2240. https://doi.org/10.5194/acp-9-2227-2009

Hatch, L. E., Luo, W., Pankow, J. F., Yokelson, R. J., Stockwell, C. E., & Barsanti, K. C. (2015). Identification and quantification of gaseous organic compounds emitted from biomass burning using two-dimensional gas

chromatography–time-of-flight mass spectrometry. *Atmospheric Chemistry and Physics*, *15*(4), 1865–1899. https://doi.org/10.5194/acp-15-1865-2015

Hatch, Lindsay E, Yokelson, R. J., Stockwell, C. E., Veres, P. R., Simpson, I. J., Blake, D. R., et al. (2017). Multi-instrument comparison and compilation of non-methane organic gas emissions from biomass burning and implications for smoke-derived secondary organic aerosol precursors. *Atmospheric Chemistry and Physics*, 1471–1489. https://doi.org/10.5194/acp-17-1471-2017

Hecobian, A., Liu, Z., Hennigan, C. J., Huey, L. G., Jimenez, J. L., Cubison, M. J., et al. (2011). Comparison of chemical characteristics of 495 biomass burning plumes intercepted by the NASA DC-8 aircraft during the ARCTAS/CARB-2008 field campaign. *Atmospheric Chemistry and Physics*, *11*(24), 13325–13337. https://doi.org/10.5194/acp-11-13325-2011

Hennigan, C J, Miracolo, M. A., Engelhart, G. J., May, A. A., Presto, A. A., Lee, T., & Sullivan, A. P. (2011). Chemical and physical transformations of organic aerosol from the photo-oxidation of open biomass burning emissions in an environmental chamber, 7669–7686. https://doi.org/https://doi.org/10.5194/acp-11-7669-2011

Hennigan, Christopher J., Westervelt, D. M., Riipinen, I., Engelhart, G. J., Lee, T., Collett, J. L., et al. (2012). New particle formation and growth in biomass burning plumes: An important source of cloud condensation nuclei. *Geophysical Research Letters*, *39*(9), 1–5. https://doi.org/10.1029/2012GL050930

Heringa, M. F., DeCarlo, P. F., Chirico, R., Tritscher, T., Dommen, J., Weingartner, E., et al. (2011). Investigations of primary and secondary particulate matter of different wood combustion appliances with a high-resolution time-of-flight aerosol mass spectrometer. *Atmospheric Chemistry and Physics*, *11*(12), 5945–5957. https://doi.org/10.5194/acp-11-5945-2011

Jolleys, M. D., Coe, H., McFiggans, G., Taylor, J. W., O'Shea, S. J., Le Breton, M., et al. (2015). Properties and evolution of biomass burning organic aerosol from Canadian boreal forest fires. *Atmospheric Chemistry and Physics*, *15*(6), 3077–3095. https://doi.org/10.5194/acp-15-3077-2015

Jolleys, Matthew D., Coe, H., McFiggans, G., Capes, G., Allan, J. D., Crosier, J., et al. (2012). Characterizing the aging of biomass burning organic aerosol by use of mixing ratios: A meta-analysis of four regions. *Environmental Science and Technology*, *46*(24), 13093–13102. https://doi.org/10.1021/es302386v

Koss, A. R., Sekimoto, K., Gilman, J. B., Selimovic, V., Coggon, M. M., Zarzana, K. J., et al. (2018). Non-methane organic gas emissions from biomass burning: Identification, quantification, and emission factors from PTR-ToF during the FIREX 2016 laboratory experiment. *Atmospheric Chemistry and Physics*, *18*(5), 3299–3319. https://doi.org/10.5194/acp-18-3299-2018

Kroll, J. H., Lim, C. Y., Kessler, S. H., & Wilson, K. R. (2015). Heterogeneous Oxidation of Atmospheric Organic Aerosol: Kinetics of Changes to the Amount and Oxidation State of Particle-Phase Organic Carbon. *The Journal of Physical Chemistry A*, *119*(44), 10767–10783. Retrieved from http://pubs.acs.org/doi/10.1021/acs.jpca.5b06946

Liu, X., Huey, L. G., Yokelson, R. J., Selimovic, V., Simpson, I. J., Müller, M., et al. (2017). Airborne measurements of western U.S. wildfire emissions: Comparison with prescribed burning and air quality implications. *Journal of Geophysical Research*, *122*(11), 6108–6129. https://doi.org/10.1002/2016JD026315

Matthew, B. M., Middlebrook, A. M., & Onasch, T. B. (2008). Collection Efficiencies in an Aerodyne Aerosol Mass Spectrometer as a Function of Particle Phase for Laboratory Generated Aerosols. *Aerosol Science and Technology*, *42*(11), 884–898. https://doi.org/10.1080/02786820802356797

May, A. A., Lee, T., McMeeking, G. R., Akagi, S., Sullivan, A. P., Urbanski, S., et al. (2015). Observations and analysis of organic aerosol evolution in some prescribed fire smoke plumes. *Atmospheric Chemistry and Physics*, *15*(11), 6323–6335. https://doi.org/10.5194/acp-15-6323-2015

May, Andrew A., Levin, E. J. T., Hennigan, C. J., Riipinen, I., Lee, T., Collett, J. L., et al. (2013). Gas-particle partitioning of primary organic aerosol emissions: 3. Biomass burning. *Journal of Geophysical Research Atmospheres*, *118*(19), 11327–11338. https://doi.org/10.1002/jgrd.50828

Mohr, M., Matter, D., Burtscher, H., Mohr, M., & Burtscher, H. (1996). Efficient multiple charging of diesel particles by photoemission. *Aerosol Science and Technology*, *24*(1), 14–20. https://doi.org/10.1080/02786829608965348

Onasch, T. B., Trimborn, A., Fortner, E. C., Jayne, J. T., Kok, G. L., Williams, L. R., et al. (2012). Soot Particle Aerosol Mass Spectrometer: Development, Validation, and Initial Application. *Aerosol Science and Technology*, *46*(7), 804–817. https://doi.org/10.1080/02786826.2012.663948

Ortega, A M, Day, D. A., Cubison, M. J., Brune, W. H., Bon, D., Gouw, J. A. De, & Jimenez, J. L. (2013). Secondary organic aerosol formation and primary organic aerosol oxidation from biomass-burning smoke in a flow reactor during, 11551–11571. https://doi.org/10.5194/acp-13-11551-2013

Ortega, Amber M., Hayes, P. L., Peng, Z., Palm, B. B., Hu, W., Day, D. A., et al. (2016). Real-time measurements of secondary organic aerosol formation and aging from ambient air in an oxidation flow reactor in the Los Angeles area. *Atmospheric Chemistry and Physics*, *16*(11), 7411–7433. https://doi.org/10.5194/acp-16-7411-2016

Peng, Z., Day, D. A., Ortega, A. M., Palm, B. B., Hu, W., Stark, H., et al. (2016). Non-OH chemistry in oxidation flow reactors for the study of atmospheric chemistry systematically examined by modeling. *Atmospheric Chemistry and Physics*, *16*(7), 4283–4305. https://doi.org/10.5194/acp-16-4283-2016

Sekimoto, K., Koss, A. R., Gilman, J. B., Selimovic, V., Coggon, M. M., Zarzana, K. J., et al. (2018). High- and low-temperature pyrolysis profiles describe volatile organic compound emissions from western US wildfire fuels. *Atmospheric Chemistry and Physics Discussions*, (February), 1–39. https://doi.org/10.5194/acp-2018-52

Selimovic, V., Yokelson, R. J., Warneke, C., Roberts, J. M., De Gouw, J., Reardon, J., & Griffith, D. W. T. (2018). Aerosol optical properties and trace gas emissions by PAX and OP-FTIR for laboratory-simulated western US wildfires during FIREX. *Atmospheric Chemistry and Physics*, *18*(4), 2929–2948. https://doi.org/10.5194/acp-18-2929-2018

Shrivastava, M., Easter, R. C., Liu, X., Zelenyuk, A., Singh, B., Zhang, K., et al. (2015). Global transformation and fate of SOA: Implications of low-volatility SOA and gas-phase fragmentation reactions. *Journal of Geophysical Research: Atmospheres*, *120*(9), 4169–4195. https://doi.org/10.1002/2014JD022563

Shrivastava, M., Cappa, C. D., Fan, J., Goldstein, A. H., Guenther, A. B., Jimenez, J. L., et al. (2017). Recent advances in understanding secondary organic aerosol: Implications for global climate forcing. *Reviews of Geophysics*, *55*(2), 509–

559. https://doi.org/10.1002/2016RG000540

Spracklen, D. V., Mickley, L. J., Logan, J. A., Hudman, R. C., Yevich, R., Flannigan, M. D., & Westerling, A. L. (2009). Impacts of climate change from 2000 to 2050 on wildfire activity and carbonaceous aerosol concentrations in the western United States. *Journal of Geophysical Research Atmospheres*, *114*(20), 1–17. https://doi.org/10.1029/2008JDO10966

Tiitta, P., Leskinen, A., Hao, L., Yli-Pirilä, P., Kortelainen, M., Grigonyte, J., et al. (2016). Transformation of logwood combustion emissions in a smog chamber: Formation of secondary organic aerosol and changes in the primary organic aerosol upon daytime and nighttime aging. *Atmospheric Chemistry and Physics*, *16*(20), 13251–13269. https://doi.org/10.5194/acp-16-13251-2016

Tkacik, D. S., Robinson, E. S., Ahern, A., Saleh, R., Stockwell, C., Veres, P., et al. (2017). A dual-chamber method for quantifying the effects of atmospheric perturbations on secondary organic aerosol formation from biomass burning emissions. *Journal of Geophysical Research*, *122*(11), 6043–6058. https://doi.org/10.1002/2016JD025784

Vakkari, V, Beukes, J. P., Jaars, K., Josipovic, M., Venter, A. D., & Zyl, P. G. Van. (2018). Major secondary aerosol formation in southern African open biomass burning plumes. *Nature Geoscience*, *11*, 580–583. https://doi.org/10.1038/s41561-018-0170-0

Vakkari, Ville, Kerminen, V.-M., Beukes, J. P., Tiitta, P., van Zyl, P. G., Josipovic, M., et al. (2014). Rapid changes in biomass burning aerosols by atmospheric oxidation. *Geophysical Research Letters*, *41*(7), 2644–2651. https://doi.org/10.1002/2014GL059396

Virtanen, A., Joutsensaari, J., Koop, T., Kannosto, J., Yli-Pirilä, P., Leskinen, J., et al. (2010). An amorphous solid state of biogenic secondary organic aerosol particles. *Nature*, *467*(7317), 824–827. Retrieved from http://dx.doi.org/10.1038/nature09455

Westerling, A. L., Hidalgo, H. G., Cayan, D. R., & Swetnam, T. W. (2006). Warming and earlier spring increase Western U.S. forest wildfire activity. *Science*, *313*(5789), 940–943. https://doi.org/10.1126/science.1128834

Yokelson, R. J., Crounse, J. D., DeCarlo, P. F., Karl, T., Urbanski, S., Atlas, E., et al. (2009). Emissions from biomass burning in the Yucatan. *Atmospheric Chemistry and Physics*, *9*(15), 5785–5812. https://doi.org/10.5194/acp-9-5785-2009

Yuan, B., Koss, A. R., Warneke, C., Coggon, M., Sekimoto, K., & De Gouw, J. A. (2017). Proton-Transfer-Reaction Mass Spectrometry: Applications in Atmospheric Sciences. *Chemical Reviews*, *117*(21), 13187–13229. https://doi.org/10.1021/acs.chemrev.7b00325

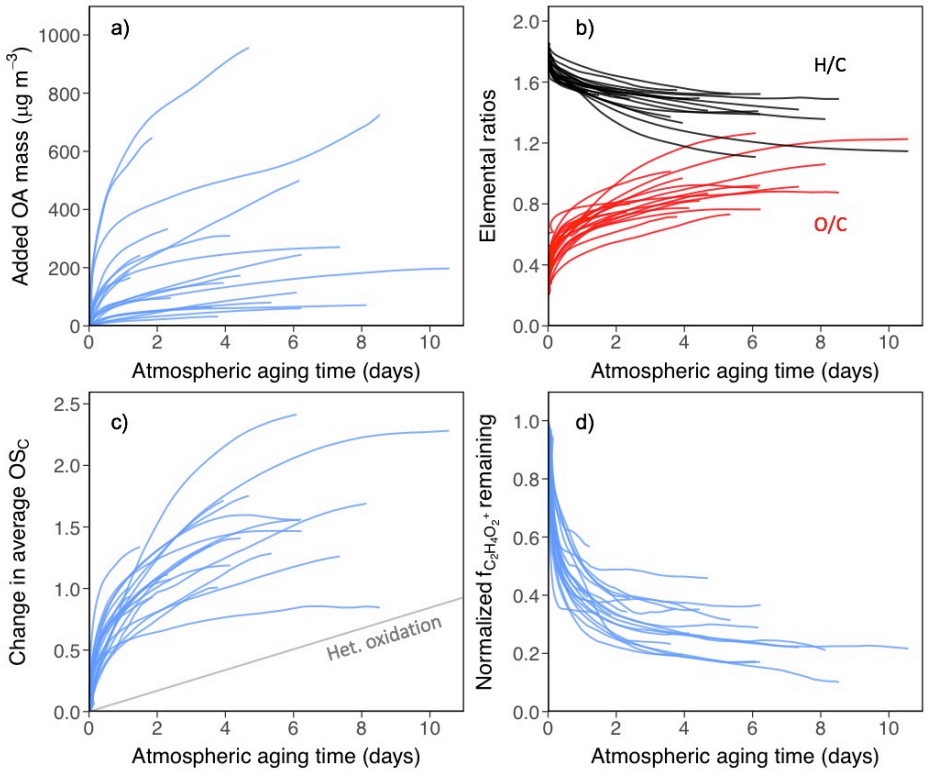

Figure 1. Changes in OA mass and composition as a function of aging time, assuming an atmospheric [OH] of 1.5 x 10^6 molec cm^{-3}. Each line represents a separate aging experiment. (a) Increase in OA mass with oxidation, showing variable SOA across all experiments. (b) Elemental ratios (red: O/C, black: H/C). (c) Change in OS_C; reference line shows average change due to heterogeneous oxidation of laboratory flow tube experiments for comparison (Kroll et al., 2015). (d) Normalized fraction of AMS organic signal due to fragment $C_2H_4O_2^+$, a common primary biomass burning OA tracer, indicative of levoglucosan and related compounds.

Deleted: average

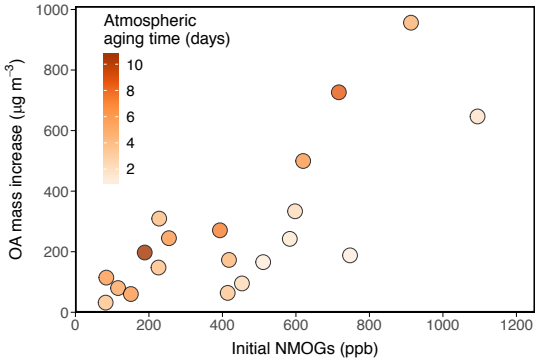

Figure 2. End-of-experiment SOA formation vs. total NMOG concentration in the chamber prior to OH oxidation. Points are colored by the atmospheric equivalent aging time corresponding to the end of each experiment.

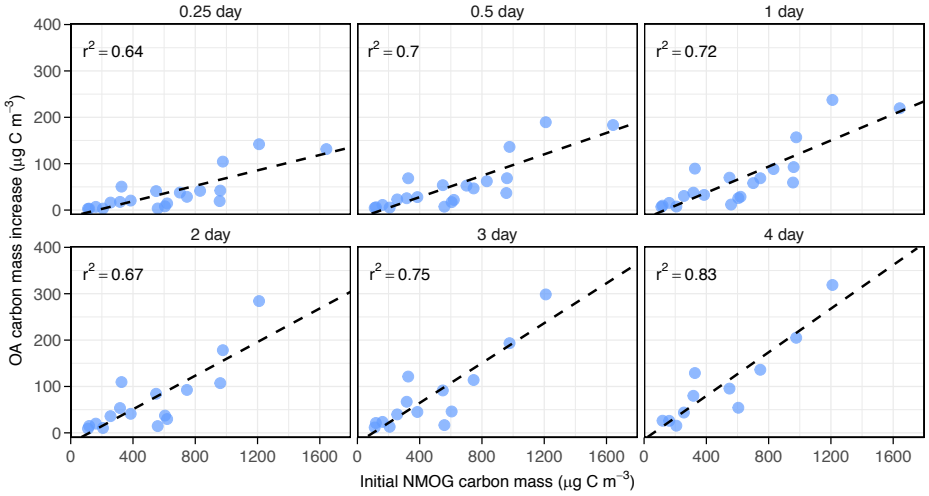

Figure 3. OA carbon mass added vs. initial NMOG carbon mass from PTR-ToF-MS measurements at various OH exposures (0.25 – 4 days of equivalent atmospheric aging). All subplots show correlation coefficients (r^2) of 0.64 or higher, and the linear relationships at longer aging times show larger slopes (i.e., more SOA; see Fig. 5).

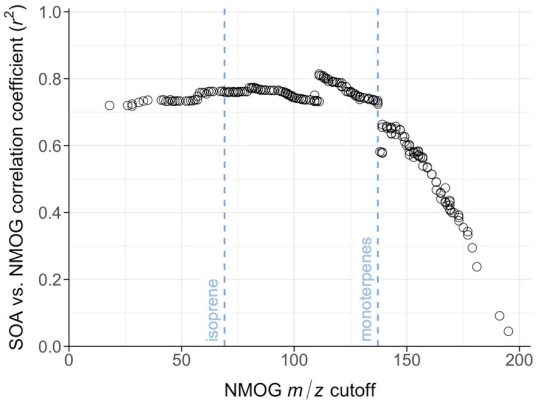

Figure 4. Correlation coefficients (r^2) between OA carbon mass added and the summed NMOG carbon mass above some ion mass (m/z) cutoff. For example, the point labeled "isoprene" shows the correlation between SOA carbon mass and initial NMOG carbon mass for all measured ions with mass-to-charge ratio equal to or greater than that of isoprene (i.e., species of molecular weight 68 g/mol or higher). Initial NMOG carbon mass is calculated prior to oxidation and data points all correspond to r^2 values at 1 day of atmospheric aging time. Correlation coefficients are high for all cutoff points below monoterpenes, then drop off due to loss of signal and the importance of compounds with lower molecular weight to SOA formation.

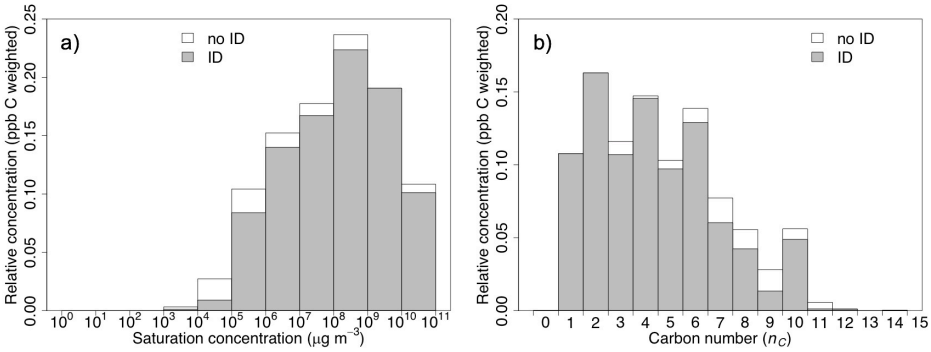

Figure 5. Estimated saturation vapor concentration distribution (a) and carbon number (n_C) distribution (b) for compounds (NMOGs) measured by the PTR-ToF-MS (Koss et al., 2018) in the chamber prior to oxidation, averaged over all burns. Distributions are separated into identified and unidentified ions and are weighted by ppb C.

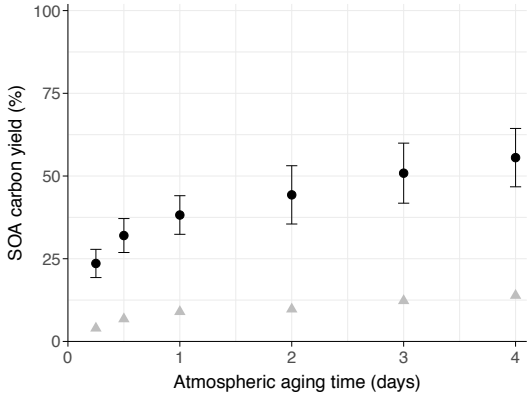

Figure 6. SOA carbon yield from aging of biomass burning emissions. Black points are carbon yields using our best estimate of OA carbon mass. Yields are calculated from the slopes of the linear relationships between SOA and initial NMOG by estimating the amount of measured NMOG carbon reacted at each respective time point using the average carbon-weighted OH rate coefficient for identified compounds and accounting for chamber dilution. Error bars are +/- 1σ in the slope of the linear fit between SOA and NMOG carbon mass. Grey triangles are estimated yields using AMS CE = 1 for all OA, both before and after aging, and is a common assumption made in previous studies on the aging of biomass burning. See Supporting Information (SI Table 2) for tabulated yields.